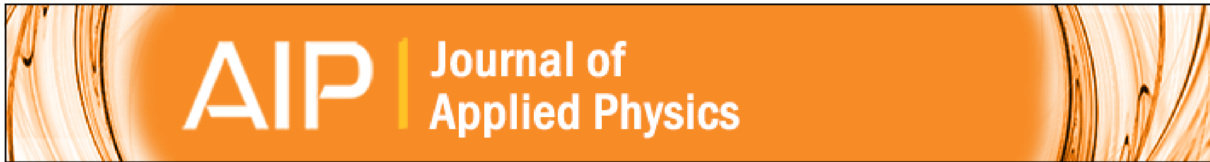

Rapid thermally annealed plasma deposited SiN_x : H thin films: Application to metal–insulator–semiconductor structures with Si, $In_{0.53}Ga_{0.47}As$, and InP

I. Mártil, A. del Prado, E. San Andrés, G. González Daz, and F. L. Martnez

Citation: Journal of Applied Physics **94**, 2642 (2003); doi: 10.1063/1.1592625
View online: http://dx.doi.org/10.1063/1.1592625
View Table of Contents: http://scitation.aip.org/content/aip/journal/jap/94/4?ver=pdfcov
Published by the AIP Publishing

Re-register for Table of Content Alerts

Create a profile.

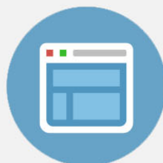

Sign up today!

[This article is copyrighted as indicated in the article. Reuse of AIP content is subject to the terms at: http://scitation.aip.org/termsconditions. Downloaded to] IP: 147.96.14.15 On: Wed, 12 Feb 2014 18:55:00

Rapid thermally annealed plasma deposited SiN_x:H thin films: Application to metal–insulator–semiconductor structures with Si, $In_{0.53}Ga_{0.47}As$, and InP

I. Mártil,[a] A. del Prado, E. San Andrés, and G. González Díaz
Dipartmento Física Aplicada III, Faculty Ciencias Físicas, University Complutense, 28040 Madrid, Spain

F. L. Martínez
Dipartmento Electrónica, Tecnología de Computadoras y Proyectos, University Politécnica de Cartagena, 30202 Cartagena, Spain

(Received 27 January 2003; accepted 27 May 2003)

We present in this article a comprehensive study of rapid thermal annealing (RTA) effects on the physical properties of SiN_x:H thin films deposited by the electron cyclotron resonance plasma method. Films of different as-deposited compositions (defined in this article as the nitrogen to silicon ratio, x=N/Si) were analyzed: from Si-rich (x=0.97) to N-rich (x=1.6) films. The evolution of the composition, bonding configuration, and paramagnetic defects with the annealing temperature are explained by means of different network bond reactions that take place depending on the as-deposited film composition. All the analyzed films release hydrogen, while Si-rich and near-stoichiometric (x=1.43) ones also lose nitrogen upon annealing. These films were used to make Al/SiN_x:H/semiconductor devices with Si, $In_{0.53}Ga_{0.47}As$, and InP. After RTA treatments, the electrical properties of the three different SiN_x:H/semiconductor interfaces can be explained, noting the microstructural modifications that SiN_x:H experiences upon annealing. © *2003 American Institute of Physics.* [DOI: 10.1063/1.1592625]

I. INTRODUCTION

For many years, the microelectronic industry has been using SiN_x:H films as a protective barrier in integrated circuit manufacturing, etch stop layers for wet and plasma etching, and to prevent oxidation of underlying silicon in the local oxidation of silicon isolation technique. As a consequence, a substantial amount of research on its physical and chemical properties has been done.[1–5] But interest in SiN_x:H has been recently expanded to its use as gate dielectric on silicon complementary metal–oxide–semiconductor (CMOS) transistors, in III–V compound semiconductor devices, and in thin film transistors (TFTs) for imaging and flat panel display applications.

In the silicon based CMOS integrated circuit industry, the necessity of finding an alternative to SiO_2 as the gate material is becoming imperative as device dimensions shrink towards the 0.1 μm range. At this channel length, oxide thickness should be in the order of 15–20 Å. Such ultrathin oxides may not be usable for the manufacture of high performance CMOS circuits due to gate leakage current through the film and the effect of boron penetration from the polysilicon gate contact. Therefore alternative high-k dielectrics are being investigated intensively.[6] Among them, SiN_x:H has produced the most promising results,[7] although its application to a manufacturing process remains to be demonstrated. In the III–V compound semiconductor industry, SiN_x:H appears as the most likely candidate as a gate dielectric for metal–insulator–semiconductor field effect transistors (MISFETs).[8,9] Finally, in the imaging and display technologies, TFTs using SiN_x:H gate dielectrics, are already widespread as switching elements in active matrix arrays.[10]

SiN_x:H thin films can be grown by thermal chemical vapor deposition (CVD) or by plasma enhanced CVD. Plasma deposited SiN_x:H films are generally amorphous, but due to the bonding constraints its structure is much more strained than SiO_2. Also, SiN_x:H deposited films contain much more hydrogen than SiO_2 films. The source of the hydrogen is SiH_4 and NH_3·precursor gases (employed in many deposition schemes). The amount of hydrogen can be as large as 20–30 at. % in conventional plasma deposited SiN_x:H films. The presence of hydrogen contributes to relax bonding constraints by lowering the average coordination number of the network. This is the reason that makes SiN_x:H films the dielectric of choice for the gate structure of TFTs.[11]

A conventional plasma CVD reactor may be appropriate for most of the less demanding applications, but due to the direct ion bombardment on the growing film it is not adequate for the production of gate dielectrics. For this purpose different alternatives have been investigated, such as remote plasma,[12] electron cyclotron resonance (ECR) plasma,[13] and jet vapor deposition.[7]

In MISFET transistors with SiN_x:H gate, such as those being investigated for Si devices and for III–V compound semiconductor devices, there are two issues of concern that at the present moment limit their performance: the high hydrogen content and the high density of interface states. On silicon devices, some different approaches have been explored to reduce the density of interface states to a level comparable to thermal oxides: stacked dielectric structures

[a]Author to whom correspondence should be addressed; electronic mail: imartil@fis.ucm.es

0021-8979/2003/94(4)/2642/12/$20.00 © 2003 American Institute of Physics

[This article is copyrighted as indicated in the article. Reuse of AIP content is subject to the terms at: http://scitation.aip.org/termsconditions. Downloaded to] IP: 147.96.14.15 On: Wed, 12 Feb 2014 18:55:00

such as oxide–nitride–oxide (O–N–O)[14] or oxide–nitride (O–N),[15] as well as nitrided oxide interfaces.[16] For III–V semiconductors, SiN_x:H seems to be preferable both to native oxides and to CVD SiO_2 because it allows the elimination of oxygen in the processing of III–V devices, and its interface properties have been substantially improved by different techniques like, for instance, the growing of an intermediate pseudomorphic silicon interface control layer (ICL).[17]

A postdeposition rapid thermal anneal (RTA) may have different effects on the SiN_x:H films depending mainly on the hydrogen content. Moderate annealing temperatures can provide the activation energy necessary to promote the passivation of defects by the formation of Si–H and N–H bonds together with a general relaxation of bonding constraints and stress, and hence produce an improvement in device performance. Higher annealing temperatures may cause hydrogen or nitrogen release. If the evolution of hydrogen brings about Si–N bond healing then the device may improve its characteristics.[14,18] On the other hand, when the release of hydrogen leaves unpassivated defects or causes a loss of nitrogen atoms, then a degradation of the performance is observed.[17]

In this article, we analyze in detail the influence of the RTA on the physical properties of ECR deposited SiN_x:H films in a wide range of compositions—from Si-rich films to N-rich—and analyze the RTA effects on the SiN_x:H/semiconductor interface with Si,[19–21] $In_{0.53}Ga_{0.47}As$,[22,23] and InP.[24–27]

II. EXPERIMENT

A. SiN_x:H deposition and characterization techniques

To perform the nonelectrical characterization of the SiN_x:H, thin films of variable composition were deposited by an ECR plasma method directly on Si wafers with (111) orientation and 80 Ω cm resistivity. The deposition reactor was an ASTEX 4500 machine operating at 2.45 GHz. The wafers had been previously sliced in square pieces of 1 cm×1 cm. The cleaning of the substrates was done using the standard RCA procedure. Immediately afterwards they were introduced in the vacuum chamber, which was pumped down to about 3×10^{-7} mbar before initiating the deposition process.

N_2 and pure SiH_4 were used as precursor gases. According to previous publications,[13,28] the composition of the SiN_x:H was controlled by the N_2 to SiH_4 gas flow ratio ($\mathbf{R}=N_2/SiH_4$). The films analyzed in this article were deposited with five different values of **R** (**R**=1, 1.6, 5, 7.5, and 9), which resulted in different compositions (defined in this article as the nitrogen to silicon ratio, $x=[N]/[Si]$). The value of x for each gase flow ratio was $x=0.97$, 1.43, 1.5, 1.55, and 1.6, respectively, as we will see in the Sec. III A of this article. Noting the film composition, the resulting films will be referred in the following as Si rich (**R**=1), near stoichiometric (**R**=1.6), and N rich (**R**=5, 7.5, and 9).

In all depositions microwave power was 100 W and the total gas flow was set at 10.5 sccm, for a pressure of 0.6 mbar. The substrate holder was unintentionally heated.

After the deposition, the SiN_x:H samples were rapid thermally annealed in Ar atmosphere at temperatures between 300 and 1050 °C for 30 s. This was done inside a graphite susceptor in a Modular Process Technology RTP-600 furnace.

The nitrogen to silicon ratio (x=N/Si) of films was determined by Rutherford backscattering spectrometry (RBS) and averaged with the value obtained by energy dispersive x-ray microanalysis (EDX). In order to study the evolution of hydrogen in the film as a function of annealing temperature we also use heavy ion elastic recoil detection analysis (HI-ERDA). Details about these characterizations can be found in Refs. 29–31.

The bonding characteristics of the films was obtained by means of Fourier transform infrared spectroscopy. The infrared spectra were recorded with a Nicolet 5PC Fourier transform spectrometer, and the density of bonded hydrogen was calculated from the area of the Si–H and N–H stretching bands applying the calibration factors obtained by Lanford and Rand.[32] The thickness of the samples was about 190 nm for the Si-rich films, 240 nm for the near-stoichiometric series, and 300 nm for the N-rich samples.

To obtain information about the type and density of paramagnetic defects present in the films, electron spin resonance (ESR) measurements were performed with a Bruker ESP 300E spectrometer operating in the X band at a microwave power of 0.5 mW. In order to obtain good signal to noise ratio, we perform the measurements on stacks of films of 1000, 2400, and 3200 nm for Si-rich, near-stoichiometric, and N-rich samples, respectively. The unique defect detected in the films was the well known Si dangling bond (also known as the K center).[5] This will be noted in this article as Si_{DB}. The density of such defect was quantified by comparison with the signal of a calibrated weak pitch standard.

B. Al/SiN_x:H/semiconducor metal–insulator–semiconductor fabrication and characterization

The electrical characterization of SiN_x:H films was performed on metal–insulator–semiconductor (MIS) devices, using three different semiconductors as substrate (Si, $In_{0.53}Ga_{0.47}As$, and InP). The deposition conditions were the same than those previously described for SiN_x:H deposition, except the substrate temperature, that was now 200 °C.[19,22,33] The thickness of the SiN_x:H film was between 20 and 50 nm. After the RTA treatments, the samples were subjected to additional processing in order to fabricate the metal contacts. The front contact in all the devices was always Al, which was thermally evaporated through a mask in order to produce several squared contacts of 1.12×10^{-3} cm^2 of area on each sample. No mask was used for the back contact, which was different for each semiconductor substrate, as we detail later. After evaporation of both front and rear contacts, a postmetallization anneal was performed at 300 °C during 20 min in a conventional furnace purged with Ar. Specific details of MIS fabrication with each type of substrate (Si, $In_{0.53}Ga_{0.47}As$, and InP) are detailed in the next paragraph.

For the Al/SiN_x:H/Si structures, the substrate was n-type Si with (100) orientation and a resistivity of 5 Ω cm.

[This article is copyrighted as indicated in the article. Reuse of AIP content is subject to the terms at: http://scitation.aip.org/termsconditions. Downloaded to] IP: 147.96.14.15 On: Wed, 12 Feb 2014 18:55:00

The Si cleaning step was the same as we have described for SiN_x:H deposition. The back contact was thermally evaporated Al. SiN_x:H film thickness was about 50 nm.

For the Al/SiN_x:H/$In_{0.53}Ga_{0.47}As$ devices, the substrates used were commercial epilayers grown by metalorganic chemical vapor deposition on (100) InP substrate. Two different kinds of ternary semiconductor have been used: n-$In_{0.53}Ga_{0.47}As$ (S doped, $n=6.6\times10^{15}\,cm^{-3}$), and p-$In_{0.53}Ga_{0.47}As$ (Zn doped, $p=1.1\times10^{16}\,cm^{-3}$). The semiconductor surface was ultrasonically degreased with organic solvents, and treated in HCl:H_2O (1:3) just before being transferred to the vacuum deposition chamber. We used AuGe/Au or AuZn/Au metallizations to form the back ohmic electrode over n-type and p-type wafers, respectively.[22,23] SiN_x:H film thickness was 50 or 20 nm in some devices.

Finally, for the Al/SiN_x:H/InP devices, wafers of unintentionally doped InP ($n=5\times10^{15}\,cm^{-3}$, (100) oriented) were used as substrate. The samples were fist degreased with organic solvents, rinsed in de-ionized water, and dried with nitrogen. They were then superficially etched in a solution of HIO_3:H_2O (10% at weight) for 1 min and in HF:H_2O (1:10) for 15 s.[26,27] Because this device was the most difficult to optimize, two different MIS structures were analyzed for optimization:

(i) In the first type, the insulator deposition was performed in two steps: the first SiN_x:H layer (bottom layer, 10 nm thick), deposited onto the InP, was chosen to have a composition of $x=1.6$ (i.e., deposited at $\mathbf{R}=9$) to minimize the interface trap density.[26,27] The second layer (top layer, 40 nm thick) was deposited at $\mathbf{R}=1.6$ ($x=1.43$) to improve the ρ and E_B values. The finalized gate structure will be referred to as dual layer.

(ii) In the second type, a N_2 plasma exposure was performed during 30 s., with a 60 W microwave power and a N_2 pressure of 0.6 mbar, followed by the deposition of a SiN_x:H single layer insulator at $\mathbf{R}=9$ ($x=1.6$).[27] Finally, an AuGe/Au back electrode was evaporated.

Once finished, the MIS devices were characterized by measuring the capacitance–voltage ($C-V$) characteristics. Both curves—high frequency (C_h, 1 MHz) and quasistatic (C_q)—were measured simultaneously with a Keithley Model 82 system, and the interface trap distribution (in the following, D_{it}) was obtained by means of the well known equation[34]

$$D_{it}=\frac{1}{q}C_{it}=\frac{1}{q}\left[\left(\frac{1}{C_q}-\frac{1}{C_{diel}}\right)^{-1}-\left(\frac{1}{C_h}-\frac{1}{C_{diel}}\right)^{-1}\right], \qquad (1)$$

where q is the electron charge and C_{diel} is the dielectric capacitance measured in accumulation.

The MIS devices were also characterized by current–voltage measurements in accumulation using the same Keithley Model 82 equipment. This allowed the calculation of the resistivity (ρ), in the region of ohmic conduction, and the breakdown field (E_B), defined as the electric field that produces a sudden and abrupt increase of current conduction through the dielectric.[19]

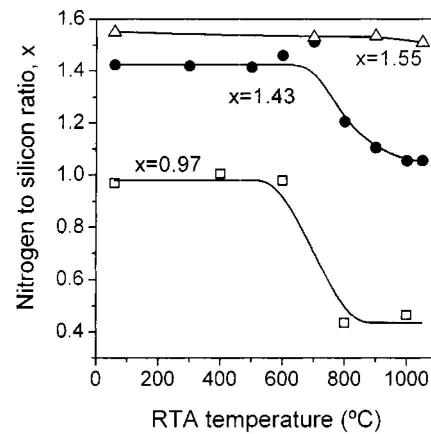

FIG. 1. Nitrogen to silicon ratio (x) of the three types of SiN_x:H films, determined by RBS and EDX, as a function of RTA temperature. Lines are a guide for the eye.

III. RESULTS AND DISCUSSION

A. RTA effects on SiN_x:H film characteristics

Figure 1 shows the average of the RBS and EDX values of the N/Si ratio (x) obtained for three representative samples of each as-deposited composition, as a function of RTA temperature. From this figure the three types of investigated films, determined by the value of the parameter $\mathbf{R}$, can be specified as follows: (i) Si-rich films grown with $\mathbf{R}=1$ having as-grown composition of $x=0.97$; (ii) near-stoichiometric films grown with $\mathbf{R}=1.6$ and having as-grown composition of $x=1.43$; and (iii) N-rich films grown with $\mathbf{R}=7.5$ having as-grown composition $x=1.55$. The films deposited at $\mathbf{R}=5$ and $\mathbf{R}=9$, have as-deposited compositions of $x=1.5$ and $x=1.6$, respectively. The behavior of these films concerning the RTA effects is the same than those deposited at $\mathbf{R}=7.5$ ($x=1.55$).

As the Si-rich and near-stoichiometric samples lose nitrogen above a certain annealing temperature (Fig. 1), we shall refer each series by the as-grown composition. From Fig. 1 the most important conclusion is that the composition of the N-rich films is essentially not affected by the RTA temperature, whereas the near-stoichiometric samples lose nitrogen above 700 °C and the Si-rich films experience a similar N loss for RTA temperatures higher than 600 °C.

Hydrogen, which is also present in the films but cannot be detected by RBS and EDX, was analyzed by HI-ERDA in the as-grown films. A typical concentration of the order of 10 at. % was obtained. The HI-ERDA measurements were found to be in good agreement with the results obtained from Si–H and N–H bonds using the calibration factors of Lanford and Rand.[30,32] For this reason, we consider use the infrared absorption band areas as reliable values of the actual hydrogen content of the films.

Three absorption bands are observed in the infrared spectra of our SiN_x:H films, corresponding to the Si–N, Si–H, and N–H stretching oscillations. We detail next the information extracted from each band.

[This article is copyrighted as indicated in the article. Reuse of AIP content is subject to the terms at: http://scitation.aip.org/termsconditions. Downloaded to] IP: 147.96.14.15 On: Wed, 12 Feb 2014 18:55:00

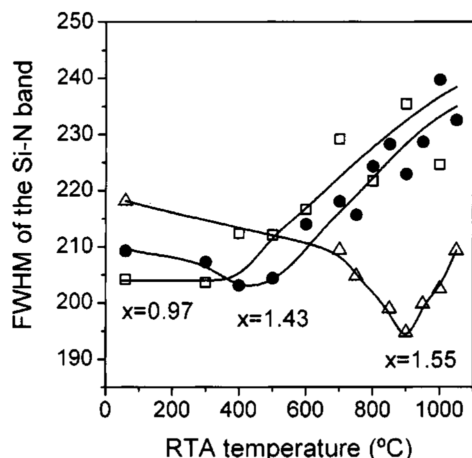

FIG. 2. Full width at half maximum of Si–N stretching absorption band as a function of RTA temperature. As-deposited film composition is showed in the figure. Lines are guides for the eye.

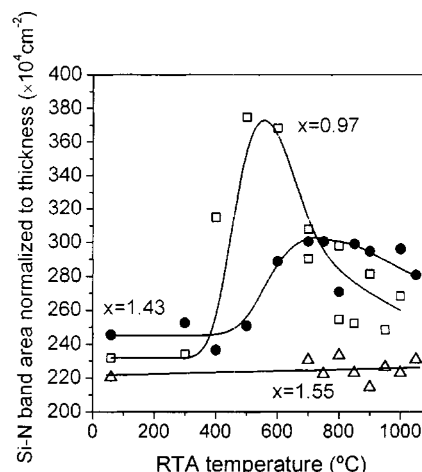

FIG. 3. Area of the Si–N band normalized to film thickness as a function of RTA temperature. As-deposited film composition is showed in the figure. Lines are drawn to guide the eye.

1. Si–N absorption band

This well-known band is due to an asymmetric stretching vibration of the Si–N bond. Depending on the near chemical neighbor environment, the maximum absorption can occur for a wave number between 750 and 970 cm^{-1}.[35–37] Besides of the dependence on the electronegativity of the surrounding atoms, the Si–N stretching band shape is also affected by the dispersion range of bond angles, which modify the vibration frequency and therefore determine the width of the band. Thus, the full width half maximum (FWHM) of the band reflects the overall disorder of the network topology, with a broader band corresponding to a higher dispersion of bond angles and, therefore, a higher disorder. Figure 2 shows the evolution of the Si–N band FWHM as a function of annealing temperature for the three types of films. A significant decrease is observed for the N-rich composition for RTA temperatures up to 900 °C, and at lower annealing temperatures also for the near-stoichiometric films, indicating a thermally activated reordering of the network, with bond angles returning to their thermodynamically most stable values. On the contrary, the films with the Si-rich composition do not experience this lattice relaxation. Above a certain temperature, depending on the composition, the band width increases indicating that some process begins to produce a structural disorder. We will next relate this process to bond reactions involving hydrogen and nitrogen release, which are suggested by the results of composition and bonded hydrogen density.

The area of the Si–N absorption band is proportional to the density of these bonds. The calibration of this band (i.e., the determination of the oscillator strength) is not as well established in the scientific literature as is the calibration of the Si–H and N–H bands to obtain the total content of hydrogen.[35] For this reason, in Fig. 3 we have plotted the area of this band versus annealing temperature without converting it to bond density. Nevertheless, within each composition series the plot indicates the trends of the Si–N bond density evolution of these films. For the Si-rich and near-stoichiometric samples there is a significant increase of Si–N bond density with annealing temperature up to 600 °C in the first case and 700 °C in the second. As we will see, this is in agreement with bond network reactions that will be considered to occur in this range of temperatures. For higher temperatures the band area decreases together with the loss of nitrogen, and as we will report in the following Figs. 5 and 6, with the loss of hydrogen.

2. Si–H and N–H absorption bands

The density of bonded hydrogen is shown in Figs. 4 and 5 for the three types of films as a function of the RTA temperature. The Si-rich and near-stoichiometric compositions exhibit both Si–H and N–H bonds, while for N-rich films only N–H bonds are found. Additionally, in as-grown films, an additional amount of hydrogen in atomic or molecular form is probably trapped in microvoids of the structure. This might explain why at moderate annealing temperatures Si–H and N–H bonds are formed and thus the density of bonded hydrogen increases in this temperature range. For higher annealing temperatures hydrogen is lost due to the breaking of Si–H and N–H bonds. We will propose a reaction model for these processes.

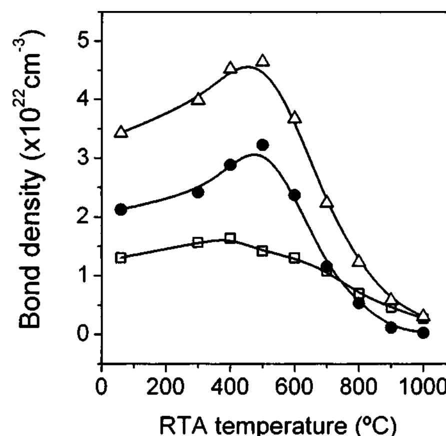

FIG. 4. Density of bonded hydrogen for Si-rich films: Si–H bonds (●); N–H bonds (□). Total content of bonded hydrogen (△). Lines are drawn as guides to the eye.

[This article is copyrighted as indicated in the article. Reuse of AIP content is subject to the terms at: http://scitation.aip.org/termsconditions. Downloaded to] IP: 147.96.14.15 On: Wed, 12 Feb 2014 18:55:00

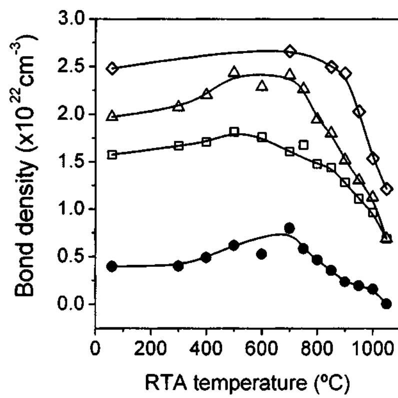

FIG. 5. Density of bonded hydrogen for the near-stoichiometric and N-rich samples as a function of RTA temperature. Near-stoichiometric films: N–H bonds (□); Si–H bonds (●), and total content of bonded hydrogen (△). N-rich films only show N–H bonds (◇). Lines are guides to the eye.

The wave number at which the maximum absorption takes place, contains information about the near-neighbor arrangements around the vibrating bond. The higher the electronegativity of the surrounding atoms, the higher is the frequency (or wave number) of the vibration. Peak absorption position of the Si–H stretching mode are shown in Fig. 6 for the Si-rich and near-stoichiometric samples, as a function of RTA temperature. The Si–H band shifts to lower wave numbers as the annealing temperature increases. For the near-stoichiometric samples this shift occurs above 700 °C, in perfect coincidence with the of nitrogen and hydrogen loss, which will be discussed in detail in the next section. For the Si-rich samples, the shift takes place between 300 and 500 °C. So, it is not related to the same process as for the near-stoichiometric composition. All these results are discussed in the following sections.

Network relaxation. It is interesting to remark the striking difference between the Si-rich samples and the other two types of films with respect to the temperature dependence of the Si–N bandwidth (see Fig. 2). While the N-rich and near-stoichiometric samples experience an initial decrease of the FWHM parameter up to an annealing temperature of 900 °C in the first case and 400–500 °C in the second, the Si-rich films do not show this behavior. The decrease of the FWHM parameter points to a thermal relaxation process whereby the distorted bond angles being present in the as-grown film network return to a stable minimum-energy configuration approaching their thermal equilibrium values. The absence of an equivalent relaxation process for the Si-rich case is attributed to a higher stress due to the higher coordination number of silicon (4) with respect to nitrogen (3). It is known that a percolation threshold exists in SiN_x:H at a composition of about $x=1.1$.[38] For values of x below $x=1.1$, i.e., for our Si-rich film series, there are continuous chains of Si–Si bonds extending throughout the whole lattice. These chains increase the connectivity of the network and make the structure very rigid and stressed because of the high coordination number of silicon. This explains why the network of these films does not experience a measurable thermal relaxation process. For the other two types of films, the as-grown composition is above the percolation threshold and therefore uninterrupted percolation chains do not exist. The network of these films has more flexibility because of the lower number of constraints present[39,40] and therefore a thermally activated relaxation process may become active.

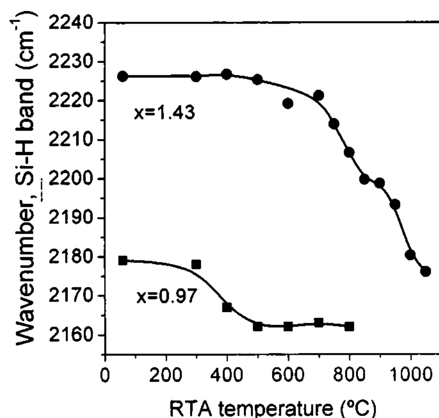

FIG. 6. Peak absorption wave number of the Si–H stretching mode for the films that present this band in the infrared spectra. Lines are drawn as guides to the eye.

This interpretation of the Si–N band width changes is in complete accordance with the results of the optical absorption edge of our films in the visible region.[41]

Hydrogen redistribution at moderate annealing temperatures. At moderate RTA temperatures, we observe that below 600 °C for the Si-rich composition and 700 °C for the near-stoichiometric films, the N/Si ratio remains constant (Fig. 1) while the content of bonded hydrogen increases in a more noticeable way the Si–H than the N–H bond concentration. Additionally, the latter begins to decrease at a lower temperature than the former. We interpret these results as an evidence for the following chemical ordering reaction taking place:

$$\text{Si–Si}+\text{N–H}\rightarrow\text{Si–H}+\text{Si–N}. \quad (2)$$

This is a well known[42] network bond process favored by the tendency to approach chemical equipartition, whereby the formation of Si–H and Si–N bonds is favored at the expense of Si–Si and N–H bonds. The formation of Si–N bonds also explains the increase of the Si–N absorption band area observed in Fig. 3. In the N-rich films this process does not take place because of the much lower density of Si–Si bonds, and therefore the Si–N band area remains unaffected by the annealing temperature and no Si–H band appears in the spectrum. A detailed analysis of how reaction (2) takes place can be found in Ref. 31, that is in agreement with the results published by other authors.[35,37,43,44]

Hydrogen release at high annealing temperatures. The Si-rich and near-stoichiometric samples experience a loss of nitrogen for temperatures higher than 600 and 700 °C, respectively (see Fig. 1), accompanied by the loss of bonded hydrogen (see Figs. 4 and 5). This does not occur for the N-rich composition where a constant N/Si ratio is maintained (Fig. 1). In the N-rich sample series the loss of bonded hydrogen occurs mainly above 900 °C (Fig. 5). The process of nitrogen and hydrogen release for the Si-rich and near-stoichiometric samples can be explained by a cooperative

[This article is copyrighted as indicated in the article. Reuse of AIP content is subject to the terms at: http://scitation.aip.org/termsconditions. Downloaded to] IP: 147.96.14.15 On: Wed, 12 Feb 2014 18:55:00

reaction between Si–H and N–H bonds, and the effusion of an ammonia fragment which is able to capture rapidly an additional hydrogen atom to form an ammonia molecule[29,31,45]

$$\text{Si–H} + \text{H–NSi–H} \rightarrow \text{Si–Si} + NH_3\uparrow. \tag{3}$$

Finally, the process of hydrogen release in the N-rich film follows a different mechanism. These samples do not exhibit any detectable loss of nitrogen in the whole range of annealing temperatures. Therefore the process of hydrogen out-diffusion cannot take place with a simultaneous release of nitrogen as described above. Since there are no detectable Si–H bonds the process can only involve N–H bonds. As a straightforward reaction to describe such process we consider[29,31]

$$\text{Si–N–H} + \text{Si–N–H} \rightarrow 2(\text{Si–N}\cdot) + H_2\uparrow. \tag{4}$$

As with the Si-rich and near-stoichiometric cases, the process also takes place with the formation of H-bonding interactions, in this case between doubly occupied hybrid sp^3 nitrogen orbitals and hydrogen atoms of a N–H group in the next vicinity. Further details of this process can be found elsewhere.[31]

A careful analysis of the activation energies (E_a) at which the hydrogen effusion takes place in the three different types of films analyzed,[31] gives the following results:

$$E_a(\text{Si rich}) = (0.950 \pm 0.016)\ \text{eV},$$

$$E_a(\text{near stoichiometric}) = (1.22 \pm 0.09)\ \text{eV},$$

$$E_a(\text{N rich}) = (2 \pm 0.19)\ \text{eV}.$$

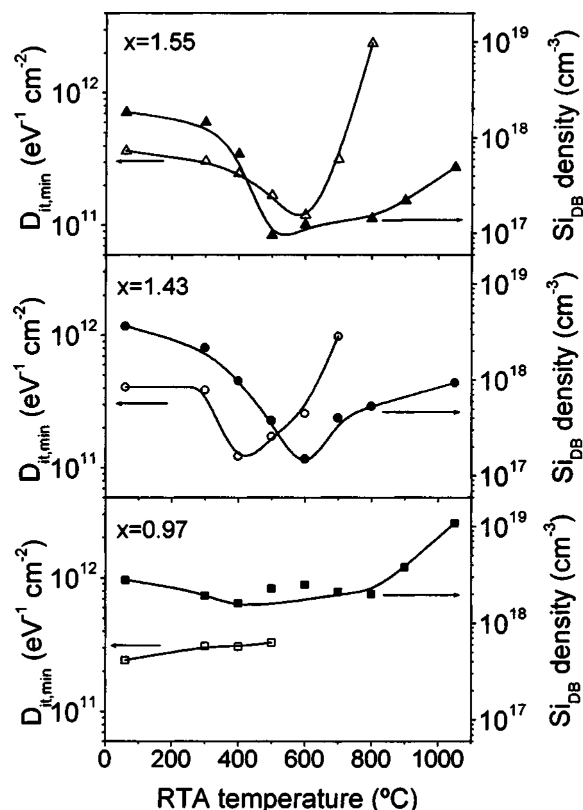

FIG. 7. Si_{DB} density (full symbols) and $D_{it,min}$ (empty symbols) as a function of RTA temperatures for the three SiN_x:H compositions: N-rich (upper graph), near-stoichiometric (middle graph), and Si-rich (lower graph). Lines are drawn as a guide for the eye.

Figure 7 shows the density of paramagnetic deffects (Si_{DB}), associated with the well known Si-dangling bond (the so-called K center)[46] for the three types of films analyzed. The trends with annealing temperature indicate a significant reduction of Si_{DB} up to 600 °C and an increase at higher temperatures, except for the Si-rich films, in which the initial decrease is much less significant. In this figure, we also show the minimum of the interface trap density ($D_{it,min}$) of Al/SiN_x:H/Si devices made with the same SiN_x:H film composition. These results will be explained in the next section

The decrease of Si_{DB} can be due to three possible causes: (i) a real disappearance of the defects as a consequence of a reconstruction of the network; (ii) a passivation by hydrogen atoms; and (iii) a charge transfer that renders the defects diamagnetic. In Figs. 4 and 5 we have already shown the thermal evolution of the bonded hydrogen content for the three types of films. As we have detailed on the previous section, in the Si-rich and near-stoichiometric samples there is an increase of the Si–H bond density up to 500 and 700 °C, respectively. Although these graphs may seem to support the hypothesis of a passivation of silicon dangling bond centers by the formation of Si–H bonds, it should be noted that a similar increase of Si–H bonds is detected for the Si-rich and near-stoichiometric samples, but the defect density does not show a comparable decrease for the Si-rich sample. This different behavior could be related to the change in N–H to Si–H bond density, as N content increases. As we have explained previously, the changes of Si–H and N–H bond density at moderate temperatures (lower than 500 °C for the Si-rich films and 700 °C for the near stoichiometric) are due to the breaking of weak Si–Si bonds accompanied by a reaction of incorporation of hydrogen trapped in microvoids of the structure, taking place simultaneously with a transfer of hydrogen from N–H to Si–H bonds according to the reaction of chemical ordering (2). In the Si-rich film, the lower proportion of N–H bonds limits the extend to which this hydrogen transfer reaction can take place and therefore can explain the less significant passivation of dangling bonds. Nevertheless, it is important to note that Si–H bonds are not observed in the N-rich films (Fig. 5).[29,31] For this reason, and due to the parallelism between the N-rich and near-stoichiometric samples with regard to the trend of Si_{DB} (Fig. 7), we propose that the observed decrease is a consequence of charge transfer between paramagnetic defects. This charge transfer would be in agreement with the negative correlation energy that it is known to be a characteristic of these centers.[47] The consequence of the negative correlation energy model is that the intermediate charge state $K^0(\uparrow)$ has more energy (is less stable) than the lower $K^+(\ )$ and higher $K^-(\uparrow\downarrow)$ charge states. The net process could then be written as

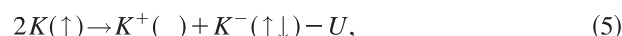

$$2K(\uparrow) \rightarrow K^+(\ ) + K^-(\uparrow\downarrow) - U, \tag{5}$$

where U is the correlation energy.

[This article is copyrighted as indicated in the article. Reuse of AIP content is subject to the terms at: http://scitation.aip.org/termsconditions. Downloaded to] IP: 147.96.14.15 On: Wed, 12 Feb 2014 18:55:00

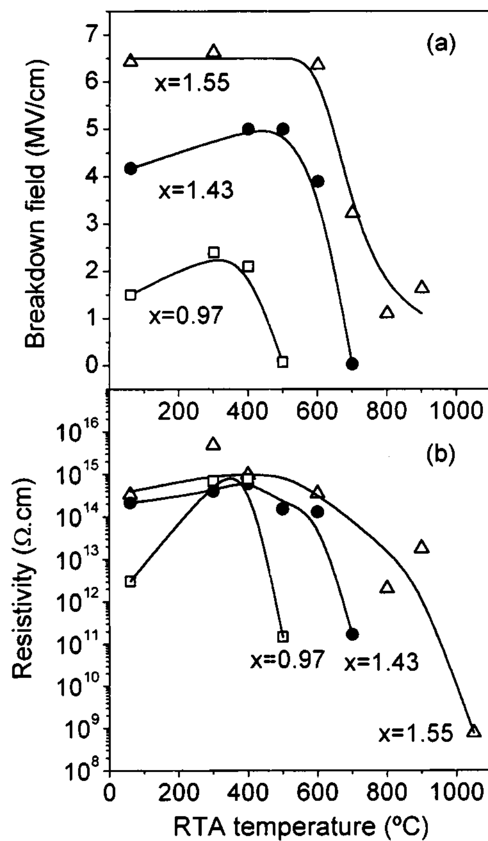

FIG. 8. (a) Breakdown field vs the RTA temperature for the Si-rich, near-stoichiometric, and N-rich films. (b) Resistivity of the three types of films as a function of RTA temperature. The lines are a guide for the eye in both cases.

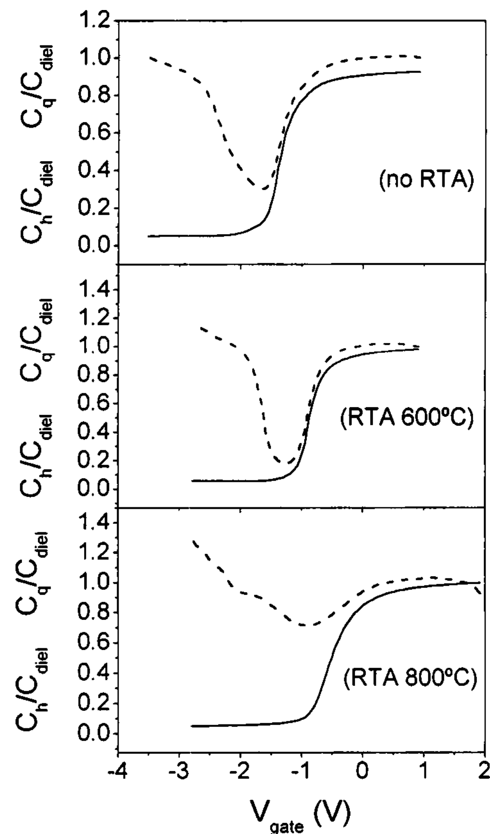

FIG. 9. High frequency (C_h, solid line) and quasistatic (C_q, dashed line) $C-V$ curves vs gate voltage, normalized to the dielectric capacitance (C_{diel}), for three devices made with N-rich films. The first device (upper graph) had no RTA treatment, while the other two were treated at the temperatures indicated in the figure.

As we have already explained, the as-grown composition of the Si-rich films is below the percolation threshold ($x=1.1$) of Si–Si bonds in the lattice of the SiN_x:H, resulting in a rigid and strained structure. This may be one of the reasons why those films do not experience the structural relaxation that takes place at moderate annealing temperatures for the other two types of films, whose as-grown composition is above the percolation limit. Results of $D_{\mathrm{it,min}}$ as a function of RTA temperature showed in Fig. 7, that we will present in the next section, seem to support this explanation.[20,41]

The increase of Si_{DB} at higher RTA temperatures is a straightforward consequence of the hydrogen release that films experience at these temperatures.

B. Al/SiN_x:H/Si devices

The values of E_B and ρ for the three series of samples analyzed are plotted in Figs. 8(a) and 8(b), respectively, versus the RTA temperature. The best electrical properties are those of the N-rich films, which have the highest values of ρ and E_B and the best thermal stability.[19,20] Although the deterioration of the near-stoichiometric films begins at 400 °C for ρ and 500 °C for E_B, acceptable values are maintained up to 600 °C. Above this temperature the deterioration process sharply arises. These results can be explained as follows: For the near-stoichiometric samples, the loss of nitrogen and bonded hydrogen above 700 °C has been already explained and modeled by means of the network reaction shown in Eq. (3). The consequence is the effusion of ammonia fragments and the formation of weak Si–Si bonds.[29] This leads to a deterioration of the values of both E_B and ρ for this type of films, as Figs. 8(a) and 8(b) evidence.

In the N-rich case, no Si–H bonds were detected in the infrared spectra and therefore the process of hydrogen release can not be the same as for the near stoichiometric samples. The N-rich films do not loose N atoms at any anneal temperature, showing a better thermal stability.[20] The loss of bonded hydrogen takes place mainly above 900 °C by the interaction of nearby N–H groups with the effusion of a hydrogen molecule [Eq. (4)]. However, at temperatures lower than this 900 °C, part of the nonbonded hydrogen trapped in microvoids of the structure may be escaping from the sample. This leaves empty cavities that produce an increase of the surface to volume ratio of the film and therefore an increase of current conduction through the dielectric, explaining the decrease of both ρ and E_B.[20]

In Fig. 9 we plot the result of a $C-V$ measurement before and after RTA processes at 600 and 800 °C for a MIS structure in which the SiN_x:H layer has N-rich composition. It is observed that the depth of the depletion dip of the quasistatic capacitance is enhanced by the annealing at 600 °C, indicating a reduction of D_{it}. When increasing the annealing temperature above 600 °C the MIS structure deteriorates,

[This article is copyrighted as indicated in the article. Reuse of AIP content is subject to the terms at: http://scitation.aip.org/termsconditions. Downloaded to] IP: 147.96.14.15 On: Wed, 12 Feb 2014 18:55:00

causing a high density of charge states at the interface and an increase of leakage current through the dielectric. Consequently, the dip of the quasistatic capacitance is less significant. Such behavior can be appreciated in the third graph of Fig. 9, corresponding to 800 °C. As we have previously shown in Fig. 8(b), the resistivity of the SiN_x:H films sharply decreases for annealing temperatures higher than 600 °C, as the material becomes a leaky insulator. This is the reason why the normalized value of the quasistatic capacitance (C_q/C_{diel}) of Fig. 9 is over 1 in the inversion zone (bias voltage lower than −2 V) for devices annealed at 600 °C (Fig. 9, middle graph) and mainly at 800 °C (Fig. 9, lower graph).[34] For the near-stoichiometric films, the behavior is qualitatively similar to that described above for the N-rich composition. Finally, the results of $C-V$ measurements performed on Si-rich samples can be found in Ref. 21.

The D_{it}, obtained from Eq. (1), always showed the characteristic U-shaped distribution, with the minimum ($D_{it,min}$) located around midgap.

As we have already detailed, Fig. 7 shows the $D_{it,min}$ as a function of RTA temperature for the three analyzed compositions of the SiN_x:H. We observe in the figure that in the N-rich and near-stoichiometric samples $D_{it,min}$ decrease up to an intermediate temperature (600 °C in the first case and 400 °C in the second). This is not observed in the Si-rich case, which experiences a moderate increase of $D_{it,min}$ up to the temperature in which the quasistatic capacitance can no longer be measured (above 500 °C).

There is an interesting parallelism between the trends that both Si_{DB} and $D_{it,min}$ follows with the RTA temperature, as Fig. 7 shows. In fact, for the N-rich composition (upper graph of Fig. 7) both parameters follow parallel trends, with a minimum at around 600 °C. Therefore this is the optimum annealing temperature. In the near-stoichiometric series, Si_{DB} also has a minimum at 600 °C, while $D_{it,min}$ have their best (lower) value at 400 °C. Finally, the trend for Si_{DB} in the Si-rich samples is almost flat up to 800 °C. A minimum value occurs at 400 °C, but we see that this minimum is much less significant than for the other two cases. Furthermore, $D_{it,min}$ has no minimum for this composition and it can only be measured up to 500 °C, showing a slightly increasing trend.[21]

From Fig. 7, we see that in the N-rich films a reduction of Si_{DB} of more than 1 order of magnitude occurs in coincidence with the reduction of $D_{it,min}$. On the near-stoichiometric composition, a similar trend is observed. In the Si-rich films, on the contrary, the minimum of Si_{DB} as a function of annealing temperature is barely significant. That means that the relaxation process that causes the decrease of Si_{DB} for the other two compositions is not acting so well for the Si-rich samples. The reason that explains the different behavior of the Si-rich films compared with the N-rich and near-stoichiometric compositions is, again, the strain caused by the percolation of Si-Si bond chains through the SiN_x:H lattice.

C. Al/SiN_x:H/$In_{0.53}Ga_{0.47}$As devices

For this type of MIS device we will first present the influence of the as-deposited SiN_x:H film composition on their electrical performance and next, the influence of RTA treatments performed on devices with exhibit the best electrical behavior before the RTA process.[23]

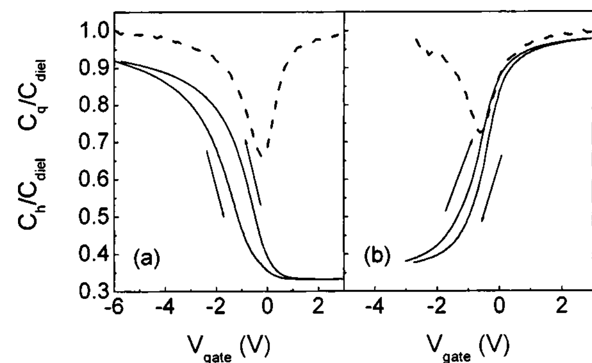

FIG. 10. High frequency (C_h, solid line) and quasistatic (C_q dashed line) $C-V$ curves vs gate voltage, normalized to the dielectric capacitance (C_{diel}), for Al/SiN_x:H/$In_{0.53}Ga_{0.47}$As capacitors: (a) p-type semiconductor; (b) n-type semiconductor. The as-deposited SiN_x:H film composition was in both cases $x=1.5$.

Figures 10(a) and 10(b) present both C_q and C_h $C-V$ curves of SiN_x:H/p-$In_{0.53}Ga_{0.47}$As and SiN_x:H/n-$In_{0.53}Ga_{0.47}$As interfaces, respectively, where the insulator film was deposited with a gas flux ratio of $\mathbf{R}=5$ (i.e., $x=1.5$). As we will see next, at this insulator composition we obtain the better SiN_x:H/$In_{0.53}Ga_{0.47}$As interface characteristics. The main differences between n-type and p-type substrates are in relation with the hysteresis values, and the frequency dispersion in the accumulation zone: the hysteresis varies from 900 meV (in the p-type MIS structure), to 240 meV (in the n-type one), whereas the frequency dispersion is about 8% and 3%, respectively. It is worth noting that these dispersion values are calculated as the relative percentage of the difference between the C_q and C_h curves in the accumulation regime. If we use a less limiting criteria (for instance, the difference between 1 kHz and 1 MHz $C-V$ curves), the dispersion measured on n-$In_{0.53}Ga_{0.47}$As MIS capacitors would be near zero, as Wang *et al.* reported.[48] From the above data, it is clear that MIS devices made on n-doped semiconductor show minor bulk insulator charge and lower D_{it} than those obtained on p-type ones.

As in the Al/SiN_x:H/Si devices, the D_{it} obtained from Eq. (1) showed in all the analyzed structures the well-known U-shaped form. Figure 11 shows $D_{it,min}$ as a function of the as-deposited SiN_x:H film composition. It is clearly seen that the $D_{it,min}$ is always better for the devices grown over an n-type semiconductor, whereas the dependence with x is almost the same for both n-type and p-type interfaces: higher values of $D_{it,min}$ are exhibited for Si-rich films or near-stoichiometric ones. As the dielectric becomes N-rich ($x \geqslant 1.5$), lower values of $D_{it,min}$ are obtained. In both cases, the values of $D_{it,min}$ measured (9.4×10^{11} cm^{-2} eV^{-1} for p-type and 6.1×10^{11} cm^{-2} eV^{-1} for n-type MIS structures) are among the lowest data reported for nonannealed *ex situ* SiN_x:H/$In_{0.53}Ga_{0.47}$As interfaces.[49]

In Fig. 12, we present E_B and ρ as a function of as-deposited SiN_x:H film composition, x, measured on both n-type and p-type SiN_x:H/$In_{0.53}Ga_{0.47}$As devices. The MIS

[This article is copyrighted as indicated in the article. Reuse of AIP content is subject to the terms at: http://scitation.aip.org/termsconditions. Downloaded to] IP: 147.96.14.15 On: Wed, 12 Feb 2014 18:55:00

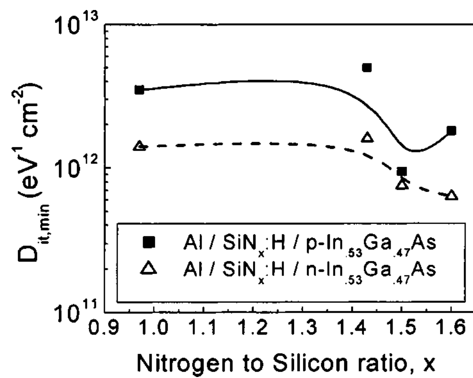

FIG. 11. $D_{\mathrm{it,min}}$ vs as-deposited SiN_x:H film composition, x, for MIS devices on p-$\mathrm{In_{0.53}Ga_{0.47}As}$ (■) and n-$\mathrm{In_{0.53}Ga_{0.47}As}$ (△). Lines are guides to the eye.

structures obtained with $\mathrm{SiN_x}$:H film with the highest nitrogen content ($x=1.6$), showed E_B higher than 4 MV/cm, that could not been measured on 50-nm-thick samples due to experimental limitations. However only for representation purposes we plot these data as 4 MV/cm on Fig. 12. On samples with thinner dielectrics ($\approx$20 nm), we have measured E_B values of 6 MV/cm. This figure indicates that both E_B and ρ increase when the film composition moves from Si rich to N rich in both n-type and p-type substrates. This behavior has already been described and explained in this article (see Fig. 8) for the SiN_x:H films deposited on Si and it is also usually found in SiN_x:H films deposited by different plasma techniques.[50,51] Such behavior is directly related to the densities of Si–H and N–H bonds present in the dielectric film.[19] As we have carefully explained in the previous section, on Si-rich samples, the concentration of Si–H bonds is high, denoting also a high concentration of Si–Si bonds. These bonds lead to an extremely rigid tetrahedral structure, promoting a high density of silicon dangling bonds that are electrically active defects. On the contrary, in N-rich films, the N–H bonds are predominant. These bonds and gives a more flexible insulator structure due to the trigonal coordination of the N bonds. As we can also see in Fig. 12, the improvement of the bulk electrical properties of the

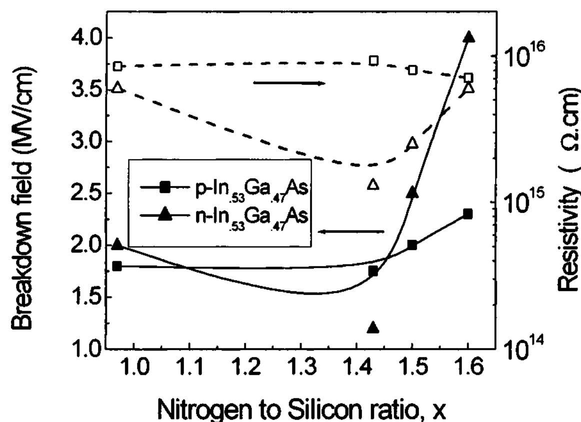

FIG. 12. Breakdown field (full symbols) and resistivity (open symbols) vs as-deposited SiN_x:H film composition, x, for p-type (■) and n-type (△) SiN_x:H/$\mathrm{In_{0.53}Ga_{0.47}As}$. Lines are guides to the eye.

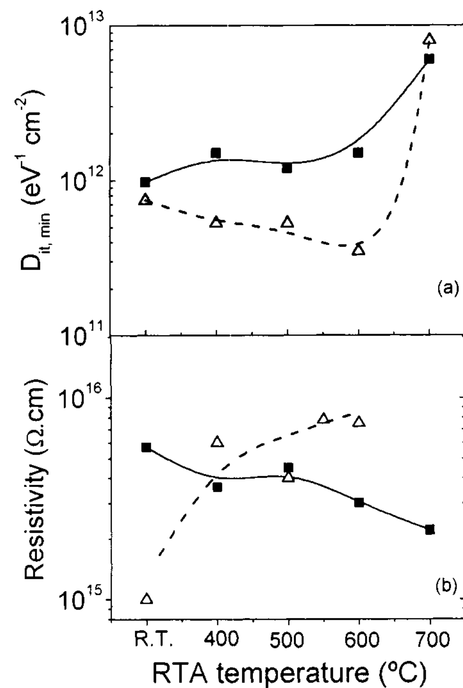

FIG. 13. (a) $D_{\mathrm{it,min}}$ vs RTA temperature, for MIS devices on p-$\mathrm{In_{0.53}Ga_{0.47}As}$ (■) and n-$\mathrm{In_{0.53}Ga_{0.47}As}$ (△). (b) Resistivity vs RTA temperature, for p-$\mathrm{In_{0.53}Ga_{0.47}As}$ (■) and n-$\mathrm{In_{0.53}Ga_{0.47}As}$ (△). As-deposited SiN_x:H film composition was $x=1.5$. Lines are guides to the eye. RT (room temperature) holds for unannealed devices.

SiN_x:H when the nitrogen content of the dielectric increase, is more significant for n-type MIS structures. On the p-type $\mathrm{In_{0.53}Ga_{0.47}As}$, the electrical properties of the dielectric are less dependent on the as-deposited film composition, showing a slight increase of E_B with x, while ρ remains almost constant at about $10^{16}\,\Omega$ cm for all the values of x analyzed.

From the previous results, we deduced that the bulk electrical properties of the SiN_x:H are dependent on the doping type of the semiconductor substrate.[51] It should be noted that the only difference between the two types of $\mathrm{In_{0.53}Ga_{0.47}As}$ epilayers used in this study is the doping element (S for the n type; Zn for the p type). The influence of the doping type on the electrical properties of the SiN_x:H/$\mathrm{In_{0.53}Ga_{0.47}As}$ structures analyzed in this work will be clarified in the next paragraphs.

Now, we will present the effect of RTA treatments on the SiN_x:H/$\mathrm{In_{0.53}Ga_{0.47}As}$ characteristics. These treatments were performed on structures in which the as-deposited SiN_x:H film composition was $x=1.5$, which results in the best SiN_x:H/$\mathrm{In_{0.53}Ga_{0.47}As}$ interface characteristics before the annealing.

In Fig. 13(a), we present a comparison between $D_{\mathrm{it,min}}$ for both n-type and p-type SiN_x:H/$\mathrm{In_{0.53}Ga_{0.47}As}$ devices, as a function of the RTA temperature. It is worth noting that there is a continuous decrease of $D_{\mathrm{it,min}}$ as the annealing temperature increase up to 600 °C for n-type MIS devices (from 7.5×10^{11} to $3.5\times10^{11}\,\mathrm{eV^{-1}\,cm^{-2}}$), and a sharp increase for higher temperatures. The behavior shown in p-type devices is quite different, because $D_{\mathrm{it,min}}$ increases from 9.5×10^{11} to $7\times10^{12}\,\mathrm{eV^{-1}\,cm^{-2}}$ as the temperature increases from 300 to 700 °C. The $D_{\mathrm{it,min}}$ obtained for the

[This article is copyrighted as indicated in the article. Reuse of AIP content is subject to the terms at: http://scitation.aip.org/termsconditions. Downloaded to] IP: 147.96.14.15 On: Wed, 12 Feb 2014 18:55:00

n-type MIS device annealed at 600 °C ($3.5\times10^{11}\,\mathrm{eV}^{-1}\,\mathrm{cm}^{-2}$) is similar to those obtained in $In_{0.53}Ga_{0.47}As$,[52] or GaAs,[53] MIS capacitors, with a Si ICL deposited between the insulator and the III–V semiconductor. Thus, from the $C-V$ measurements we conclude that an increase of the RTA temperature up to 600 °C produces a gradual improvement in the electrical quality of the interface of SiN_x:H/n-$In_{0.53}Ga_{0.47}As$ devices. On the other hand, a progressive degradation in the insulator–semiconductor interface is observed when a p-type $In_{0.53}Ga_{0.47}As$ substrate is used.

In relation with the electrical properties of the insulator, MIS devices made on p-doped substrates exhibited E_B values that increases up to 600 °C, reaching a maximum value of 3.5 MV/cm. On the other hand, on n-type substrates, E_B reaches values comprised between 7 and 8 MV/cm in the 400–600 °C range. At temperatures higher than 600 °C, E_B decreases significantly.

Concerning the resistivity, Fig. 13(b) shows ρ for n-type and p-type MIS devices, as a function of the RTA temperature. Although nonannealed p-type samples exhibit higher values of ρ than n-type ones ($6\times10^{15}\,\Omega$ cm compared to $1\times10^{15}\,\Omega$ cm), the RTA treatment induces a gradual decrease of this parameter down to $2.2\times10^{15}\,\Omega$ cm for MIS devices deposited on p-$In_{0.53}Ga_{0.47}As$, whereas on n-type substrates, an improvement of ρ up to $8\times10^{15}\,\Omega$ cm is measured. The general improvement with annealing temperature of both bulk and interface properties of n-type MIS devices has been already described in the previous section to take place also in SiN_x:H/Si interfaces and, as we have explained, it can be due to a thermal relaxation and a reconstruction of the insulator network and its interface.

Evidence of the influence of the substrate doping type on the SiN_x:H bulk properties has been presented in Figs. 12 and 13(b). In fact, both E_B and ρ are lower for p-type than for n-type annealed structures. Similar result, concerning E_B, was found by Hugon *et al.* in Al/SiN_x:H/Si structures[51] deposited by distributed ECR. These authors attributed the lower critical fields obtained in p-type MIS devices, compared to the n-type ones, to the net fixed charge density that depends on MIS structures.

There are no references in the literature in relation with anomalous diffusion of S impurities in $In_{0.53}Ga_{0.47}As$. However, it is well known the Zn-diffusion problems exist in III–V semiconductor technology.[54,55] The diffusion of Zn impurities from the semiconductor bulk towards the SiN_x:H/$In_{0.53}Ga_{0.47}As$ interface during the annealing step could conduct to poorest insulator–semiconductor interfaces, explaining the higher values of $D_{\mathrm{it,min}}$ obtained in p-type MIS devices compared with the n-type ones. On the other hand, a possible Zn loss through the insulator could explain the degradation of the resistivity with annealing temperature observed in Zn-doped structures. Therefore, we tentatively conclude that the postdeposition RTA treatment does not improve the interface and bulk properties of MIS structures deposited on the Zn-doped $In_{0.53}Ga_{0.47}As$ semiconductor.

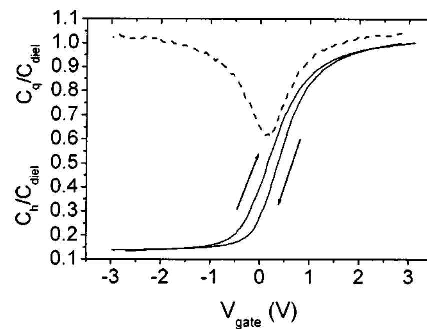

FIG. 14. High-frequency (C_h, solid line) and quasistatic (C_q, dashed line) $C-V$ curves, normalized to the dielectric capacitance (C_{diel}) of Al/$SiN_{1.5}$:H/$SiN_{1.6}$:H/InP dual-layer gate structure after annealing at 500 °C during 30 s.

D. Al/SiN_x:H/InP devices

We will first analyze results on dual-layer gate structures. In preliminary works,[25] we have shown that an inverse correlation between the value of x and $D_{\mathrm{it,min}}$ holds. The $D_{\mathrm{it,min}}$ value ($3\times10^{12}\,\mathrm{eV}^{-1}\,\mathrm{cm}^{-2}$) was achieved in films with the maximum value of x ($x=1.6$). For this composition, ρ and E_B were, respectively, $10^{15}\,\Omega$ cm and 2 MV/cm. Better insulator properties ($\rho=4\times10^{15}\,\Omega$ cm and $E_B=2.5$ MV/cm) were obtained with lower x values ($x=1.43$). However, at this insulator composition, the interface quality was worse than with $x=1.6$, now being $D_{\mathrm{it,min}}=4\times10^{12}\,\mathrm{eV}^{-1}\,\mathrm{cm}^{-2}$.

Taking into account these previous results, we have done dual-layer gate structures[26] to combine the lower interface trap densities of $SiN_{1.6}$:H compositions and the best insulator characteristics of the $SiN_{1.43}$:H or $SiN_{1.5}$:H compositions. The behavior of both ρ and E_B with the RTA treatment was similar to that shown in Fig. 8 for SiN_x:H/Si structures.

Focusing on the interface quality of these structures, in Fig. 14 the $C-V$ characteristics for Al/$SiN_{1.5}$:H/$SiN_{1.6}$:H/InP structures were annealed at 500 °C during 30 s, which is the best structure obtained. The quasistatic C_q curve presents a deep and well-defined dip, indicating the high quality of the insulator/semiconductor interface. In Fig. 15(a), we present D_{it} for the following devices: single layer Al/$SiN_{1.6}$:H/InP annealed at 500 °C/30 s; dual-layer Al/$SiN_{1.5}$:H/$SiN_{1.6}$:H/InP annealed at 500 °C/30 s; single layer Al/$SiN_{1.6}$:H/InP subjected to a N_2 plasma exposure before the SiN_x:H deposition, and finally, the same device but after annealing at 500 °C/30 s. In all the cases, D_{it} has the characteristic U-shaped form. For the RTA annealed dual-layer gate structure, the distribution exhibits a minimum ($9\times10^{11}\,\mathrm{eV}^{-1}\,\mathrm{cm}^{-2}$) located at 0.45 eV above midgap. The N_2 plasma exposure of the InP surface gives a value of $D_{\mathrm{it,min}}=1.6\times10^{12}\,\mathrm{cm}^{-2}\,\mathrm{eV}^{-1}$. The effects of the N_2 plasma exposure together with an annealing treatment has been demonstrated[27] not to be a good option to optimize the device. In fact, the device exposed to the N_2 plasma and then annealed at 500 °C during 30 s exhibited a $D_{\mathrm{it,min}}$ of $3\times10^{12}\,\mathrm{eV}^{-1}\,\mathrm{cm}^{-2}$. The thermal treatment induces the desorption of phosphorous–nitrogen (P–N) and/or indium–phosphorous–nitrogen (In–P–N) complexes probably formed on InP during the plasma cleaning, that passivate the

[This article is copyrighted as indicated in the article. Reuse of AIP content is subject to the terms at: http://scitation.aip.org/termsconditions. Downloaded to] IP: 147.96.14.15 On: Wed, 12 Feb 2014 18:55:00

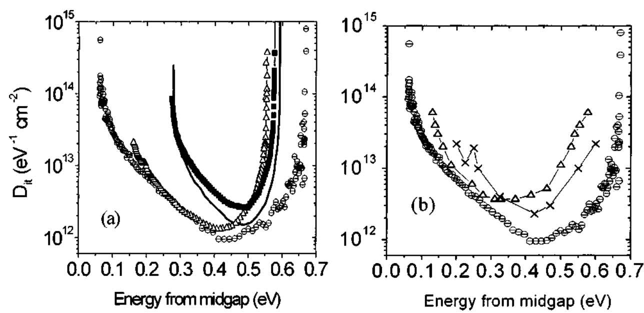

FIG. 15. (a) D_{it} as a function of gap energy plotted relative to the midgap, for the following devices: dual-layer structure of Fig. 14 (⊖); (△) single-layer $Al/SiN_{1.6}:H/InP$ annealed at 500 °C/30 s; (—) single layer $Al/SiN_{1.6}:H/InP$ subjected to N_2 plasma exposure; (■) single-layer $Al/SiN_{1.6}:H/InP$ plasma exposed and annealed at 500 °C/30 s. (b) Interface trap distribution as a function of gap energy plotted relative to the midgap, for the MIS structure showed in Fig. 14 (⊖). (△) results from Landheer *et al.* (Ref. 57) for devices passivated with an ICL, and (**X**) results from Kapila *et al.* (Ref. 58) for devices treated in H_2S atmosphere.

InP surface.[56] This desorption process gives the InP surface unpassivated and, as a consequence, the $D_{it,min}$ increases

With the comparison of data showed in Fig. 15(a), we prove that the best solution to obtain gate quality MIS devices is to use the dual-layer structure, as a gate insulator, with a RTA treatment of 500 °C during 30 s. This optimized device presents the lowest $D_{it,min}$

To compare our results with those procedures that use chemical passivation and/or ICLs to improve the interface behavior, we present in Fig. 15(b) the best D_{it} distribution obtained in this work ($Al/SiN_{1.5}:H/SiN_{1.6}:H/InP$ dual-layer gate structure annealed at 500 °C/30 s), the results from Landheer *et al.*[57] obtained in MIS structures passivated using an Si ICL and the results from Kapila *et al.*,[58] where the InP surface was treated in H_2S plasma. The $D_{it,min}$ value in our structure (9×10^{11} eV^{-1} cm^{-2}), facing those obtained with S passivation (2.5×10^{12} eV^{-1} cm^{-2})[58] or ICL technique (4×10^{12} eV^{-1} cm^{-2}),[57] indicates the excellent performance of the RTA treated dual-layer gate interface without any additional treatment of the InP surface previously to the $SiN_x:H$ deposition. These dual layer gate structures were successfully used by us to make MISFET devices with good performance.[59]

IV. CONCLUSIONS

We have shown in this article the influence of RTA processes on the physical properties of $SiN_x:H$ films deposited by the ECR plasma method. Three different types of films were analyzed: N-rich, near-stoichiometric, and Si-rich ones. In the lower range of annealing temperatures, the Si-rich or near-stoichiometric films experience an interchange bond reaction whereby Si–H and Si–N bonds are favored at the expense of N–H and Si–Si bonds. At higher annealing temperatures a loss of nitrogen is detected, which is explained together with the effusion of hydrogen by the formation of ammonia fragments. In the N-rich films no loss of nitrogen is detected at any annealing temperature, and the loss of bonded hydrogen takes place mainly above 900 °C. The breaking of the N–H bonds takes place with the formation of molecular hydrogen.

On the other hand, the RTA processes induce a thermally activated charge transfer between paramagnetic defects in the $SiN_x:H$ films for temperatures up to 600 °C when the composition is above the percolation threshold, $x=1.1$. This is observed as a considerable decrease of the density of Si_{DB} defects detected by ESR. In the samples in which Si–H bonds can be detected, this process takes place simultaneously with chemical reactions of hydrogen bond formation. The exception are the films in which percolation of Si–Si bonds occurs in the lattice. In that case the network is too rigid and does not permit defect relaxation. For higher annealing temperatures the film experiences an increase of the density of Si_{DB}, due to the loss of hydrogen.

In relation with MIS devices, for $Al/SiN_x:H/Si$ structures, in the N-rich and near-stoichiometric cases, the density of Si_{DB} and $D_{it,min}$ experience a significant decrease up to an intermediate annealing temperature. The thermal relaxation of the strain of the $SiN_x:H$ lattice at moderate annealing temperatures produces a significant decrease of $D_{it,min}$. On the contrary, the rigidity of the Si-rich structure impedes this relaxation process, and $D_{it,min}$ increases in this case from the lower annealing temperatures. For higher annealing temperatures, the release of hydrogen promoted the degradation of the electrical characteristics. As a consequence, both ρ and E_B decrease, and the leakage current through the insulator increases. The $SiN_x:H$ network is damaged by this process and both $D_{it,min}$ and Si_{DB} increases.

Regarding $Al/SiN_x:H/In_{0.53}Ga_{0.47}As$ structures, the as-deposited $SiN_x:H$ film composition plays a significant role in the interface and bulk properties of both $SiN_x:H/n\text{-}In_{0.53}Ga_{0.47}As$ and $SiN_x:H/p\text{-}In_{0.53}Ga_{0.47}As$, with better values of D_{it}, ρ, and E_B on those devices deposited with N-rich films. The bulk properties of the $SiN_x:H$ are clearly dependent on the semiconductor type doping. In general, MIS devices grown on *n*-type $In_{0.53}Ga_{0.47}As$ present higher electrical performance than *p*-type ones, even after RTA treatments.

Finally, on $Al/SiN_x:H/InP$ devices, we have shown that the dual-layer gate structure $Al/SiN_{1.5}:H/SiN_{1.6}:H/InP$ has interface properties of device quality that allows us to use such structure as the gate zone in MISFET devices. In the dual-layer gate structure, the optimization of the device with RTA treatments performed at 500 °C during 30 s gives $D_{it,min}$ of 9×10^{11} eV^{-1} cm^{-2}. This is one of the best reported values for this parameter in MIS devices with InP.

ACKNOWLEDGMENTS

The authors gratefully acknowledge Dr. M. N. Blanco and Dr. E. Redondo for the fruitful collaboration with them in recent years. They also wish to express their deep gratitude to Dr. B. Selle, Dr. I Sieber, Dr. W. Bohne, Dr. J. Röhrich, Dr. Kliefoth, Dr. W. Füssel, and in general, to the people of the Hahn-Meitner Institut in Berlin, for a long friendship and fruitful collaboration. Thanks are also due to Professor F. López and Professor D. Bravo (Materials De-

[This article is copyrighted as indicated in the article. Reuse of AIP content is subject to the terms at: http://scitation.aip.org/termsconditions. Downloaded to] IP: 147.96.14.15 On: Wed, 12 Feb 2014 18:55:00

partment, Autónoma University of Madrid) for ESR measurements. Last, but no least, technical assistance received from the people of the ion implantation facility "CAI—Implantación Iónica" of the Complutense University of Madrid (P. Fernandez and R. Cimas) is greatly acknowledge. The financial support of this work was partially done by the Spanish National Office for Science and Technology under Grant Nos. TIC 98-0740 and TIC 2001-1253

[1] E. A. Davis, N. Piggins, and S. C. Bayliss, J. Phys. C **20**, 4415 (1987).
[2] A. D. Stewart and D. L. Jones, Philos. Mag. B **57**, 431 (1988).
[3] S. Hasegawa, M. Matsuda, and Y. Kurata, Appl. Phys. Lett. **58**, 741 (1991).
[4] J. Robertson, Philos. Mag. B **63**, 47 (1991).
[5] W. L. Warren, J. Kanicki, F. C. Rong, and E. H. Poindexter, J. Electrochem. Soc. **139**, 880 (1992).
[6] G. D. Wilk, R. M. Wallace, and J. M. Anthony, J. Appl. Phys. **89**, 5243 (2001).
[7] T. P. Ma, IEEE Trans. Electron Devices **45**, 680 (1998).
[8] Z. Chen and D. Gong, J. Appl. Phys. **90**, 4205 (2001).
[9] P. N. K. Deenapanray, A. Martin, and C. Jagadish, Appl. Phys. Lett. **79**, 2561 (2001).
[10] S. S. He, M. J. Williams, D. J. Stephens, and G. Lucovsky, J. Non-Cryst. Solids **164–166**, 731 (1993).
[11] Y. Kuo, J. Electrochem. Soc. **142**, 186 (1995).
[12] Y. Yu and G. Lucovsky, IEEE Electron Device Lett. **19**, 367 (1998).
[13] S. García, J. M. Martín, M. Fernández, I. Mártil, and G. González-Díaz, Philos. Mag. B **73**, 487 (1996).
[14] Y. Ma, T. Yasuda, and G. Lucovsky, Appl. Phys. Lett. **64**, 2226 (1994).
[15] C. G. Parker, G. Lucovsky, and J. R. Hauser, IEEE Electron Device Lett. **19**, 106 (1998).
[16] G. Lucovsky, J. Vac. Sci. Technol. A **16**, 356 (1998).
[17] D. G. Park *et al.*, J. Vac. Sci. Technol. B **14**, 2674 (1996).
[18] C. Boehme and G. Lucovsky, J. Appl. Phys. **88**, 6055 (2000); J. Vac. Sci. Technol. A **19**, 2622 (2001).
[19] F. L. Martínez, A. Del Prado, E. San Andrés, I. Mártil, D. Bravo, and F. López, J. Appl. Phys. **90**, 1573 (2001).
[20] F. L. Martínez, A. del Prado, D. Bravo, F. López, I. Mártil, and G. González-Díaz, J. Vac. Sci. Technol. A **17**, 1280 (1999).
[21] F. L. Martínez, A. del Prado, I. Mártil, G. González-Díaz, K. Kliefoth, and W. Füssel, Semicond. Sci. Technol. **16**, 534 (2001).
[22] M. N. Blanco, E. Redondo, I. Mártil, and G. Gonzalez Díaz, Semicond. Sci. Technol. **14**, 628 (1999).
[23] M. N. Blanco, E. Redondo, I. Mártil, and G. González Díaz, Semicond. Sci. Technol. **15**, 823 (2000).
[24] H. Castán, S. Dueñas, J. Barbolla, N. Blanco, I. Mártil, and G. González-Díaz, Jpn. J. Appl. Phys., Part 1 **40**, 4479 (2001).
[25] E. Redondo, N. Blanco, I. Mártil, and G. Gonzalez, Appl. Phys. Lett. **74**, 991 (1999).
[26] E. Redondo, N. Blanco, I. Mártil, G. Gonzalez Díaz, R. Pelaez, S. Dueñas, and H. Castán, J. Vac. Sci. Technol. A **17**, 2178 (1999).
[27] E. Redondo, I. Mártil, G. González-Díaz, H. Castán, and S. Dueñas, J. Vac. Sci. Technol. B **19**, 186 (2001).
[28] S. García, J. M. Martín, I. Mártil, and G. González Díaz, Thin Solid Films **315**, 22 (1998).
[29] F. L. Martinez, I. Mártil, G. Gonzalez Diaz, B. Selle, and I. Sieber, J. Non-Cryst. Solids **227–300**, 523 (1998).
[30] W. Bohne, W. Fuhs, J. Röhrich, B. Selle, G. González-Díaz, I. Mártil, F. L. Martinez, and A. del Prado, Surf. Interface Anal. **30**, 534 (2000).
[31] F. L. Martínez, A. Del Prado, I. Mártil, G. González Díaz, W. Bohne, W. Fuhs, J. Röhrich, B. Selle, and I. Sieber, Phys. Rev. B **63**, 245320 (2001).
[32] W. A. Lanford and M. J. Rand, J. Appl. Phys. **49**, 2473 (1978).
[33] S. Dueñas, R. Pelaez, E. Castan, R. Pinacho, L. Quintanilla, J. Barbolla, I. Mártil, and G. Gonzalez Diaz, Appl. Phys. Lett. **71**, 826 (1997).
[34] E. H. Nicollian and J. R. Brews, *MOS (Metal Oxide Semiconductor) Physics and Technology* (Wiley, New York, 1982).
[35] E. Bustarret, M. Bensuoda, M. C. Habrad, J. C. Bruyère, S. Poulin, and S. C. Gujrathi, Phys. Rev. B **38**, 8171 (1988).
[36] S. Hasegawa, H. Anbutsu, and Y. Kurata, Philos. Mag. B **59**, 365 (1989).
[37] G. Lucovsky, J. Yang, S. S. Chao, J. E. Tyler, and W. Czubatyj, Phys. Rev. B **28**, 3234 (1983).
[38] J. Robertson, Philos. Mag. B **69**, 307 (1994).
[39] G. Lucovsky and J. C. Phillips, J. Non-Cryst. Solids **227–230**, 1221 (1998).
[40] H. He and M. F. Thorpe, Phys. Rev. Lett. **54**, 2107 (1985).
[41] F. L. Martínez, A. del Prado, I. Mártil, G. Gonzalez Díaz, B. Selle, and I. Sieber, J. Appl. Phys. **86**, 2055 (1999).
[42] Z. Yin and F. W. Smith, Phys. Rev. B **43**, 4507 (1991).
[43] B. Abeles, L. Yang, P. D. Persons, H. S. Stasiswski, and W. Lanford, Appl. Phys. Lett. **48**, 168 (1986).
[44] G. Lucovsky, R. J. Nemanich, and J. C. Knights, Phys. Rev. B **19**, 2064 (1979).
[45] K. Zellama, L. Chahed, P. Sládek, M. L. Thèye, J. H. von Bardeleben, and P. Roca i Cabarrocas, Phys. Rev. B **53**, 3804 (1996).
[46] D. T. Krick, P. M. Lenahan, and J. Kanicki, Phys. Rev. B **38**, 8226 (1988).
[47] W. L. Warren, J. Kanicki, F. C. Rong, and E. H. Poindexter, J. Electrochem. Soc. **139**, 880 (1992).
[48] Z. Wang, D. M. Diatezua, D. G. Park, Z. Chen, H. Morkoç, and A. Rockett, J. Vac. Sci. Technol. B **17**, 2034 (1999).
[49] D. S. L. Mui, Z. Wang, and H. Morkoç, Thin Solid Films **231**, 107 (1993).
[50] M. Tao, D. Park, S. N. Mohammad, D. Li, A. E. Botchkerav, and H. Morkoç, Philos. Mag. B **73**, 723 (1996).
[51] M. C. Hugon, F. Delmotte, B. Agius, and J. L. Courant, J. Vac. Sci. Technol. A **15**, 3143 (1997).
[52] Z. Wang, D. S. L. Mui, A. L. Demirel, D. Biswas, J. Reed, and H. Morkoç, Appl. Phys. Lett. **61**, 1826 (1992).
[53] D. G. Park, Z. Wang, H. Morkoc, S. A. Alterovitz, D. J. Smith, and S.-C. Tsen, J. Vac. Sci. Technol. B **16**, 3032 (1998).
[54] K. Kurishima, T. Kobayashi, and U. Gösele, Appl. Phys. Lett. **60**, 2496 (1992).
[55] S. J. Taylor, B. Beaumont, and J. C. Guillaume, Semicond. Sci. Technol. **8**, 643 (1993).
[56] M. Losurdo, P. Capezutto, G. Bruno, G. Leo, and E. Irene, J. Vac. Sci. Technol. A **17**, 2194 (1999).
[57] D. Landheer, G. Yousefi, J. B. Weeb, R. Kwok, and W. Lau, J. Appl. Phys. **75**, 3516 (1994).
[58] A. Kapila, X. Si, and V. Malhotra, Appl. Phys. Lett. **62**, 2259 (1993).
[59] E. Redondo, I. Mártil, G. González Díaz, P. Fernandez, and R. Cimas, Semicond. Sci. Technol. **17**, 672 (2002).

[This article is copyrighted as indicated in the article. Reuse of AIP content is subject to the terms at: http://scitation.aip.org/termsconditions. Downloaded to] IP: 147.96.14.15 On: Wed, 12 Feb 2014 18:55:00